Ab Initio Studies of the Electronic Structure and Geometry of UF_5 Using Relativistic Effective Core Potentials

Willard R. Wadt* and P. Jeffrey Hay

Contribution from the Theoretical Division, University of California, Los Alamos Scientific Laboratory, Los Alamos, New Mexico 87545.
Received February 20, 1979

Abstract: Ab initio calculations on the low-lying electronic states of UF_5 are presented using a relativistic effective core potential (ECP) for uranium and a nonrelativistic ECP for fluorine. The ground-state geometry of UF_5 was optimized at the SCF level using a double-ζ quality Gaussian basis set. Without spin–orbit coupling the square pyramidal structure (C_{4v}) was calculated to be 1 kcal/mol lower than the trigonal bipyramid (D_{3h}), which was subject to a Jahn–Teller distortion. Inclusion of spin–orbit effects reversed the ordering with the D_{3h} structure 1 kcal/mol lower than the C_{4v}. The two geometries are connected by a monotonic C_{2v} path, so that UF_5 will be fluxional. The ramifications of this fluxional behavior are considered. Improved virtual orbital calculations show that UF_5 has a series of weak low-lying ($2\text{–}15 \times 10^3$ cm^{-1}) f–f transitions. The results of the photofragment spectra of UF_6 are discussed in light of these calculations.

I. Introduction

Inorganic photochemistry is still a relatively unexplored field when compared to organic photochemistry. However, the rapid development of lasers together with the search for new catalysts,[1] more efficient photovoltaic devices,[2] and solar fuels[3] has greatly increased research in inorganic photochemistry. Nevertheless, very little is known about the reactive intermediates that are produced when a metal complex is photolyzed. Our ignorance is particularly apparent when one considers the paucity of reliable theoretical calculations in this area. A few ab initio studies have recently appeared for some photochemical intermediates involving transition metals, e.g., $Cr(CO)_5$.[4] However, until now no results have been reported for compounds involving the heavier transition metals, the lanthanides, or the actinides.

A new technique, relativistic effective core potentials (ECP), has been developed by Kahn, Hay, and Cowan,[5] which enables one to perform electronic structure calculations on molecules containing very heavy atoms using standard ab initio techniques. In the past, ab initio calculations on heavy-atom molecules were impractical because (1) the cost increases as N^4 where N is the number of electrons and (2) relativistic effects become so important that use of the nonrelativistic Hamiltonian leads to large errors. The first problem has been attacked for many years by constructing an effective one-electron potential that replaces the effect of the chemically inert core electrons.[6] One of the most successful approaches for ECPs,[6] which was based on numerical Hartree-Fock atomic wave functions, was well suited for inclusion of relativistic effects. By deriving the ECP from relativistic numerical atomic wave functions one can readily incorporate the important relativistic effects. Two equally successful approaches have been developed: one[7] is based on Dirac–Hartree–Fock (DHF) wave functions[8] and the other[5] is based on the approximate relativistic Hartree–Fock atomic wave functions of Cowan and Griffin.[9] The method of Ermler, Lee, and Pitzer[7] has the advantage of being more rigorous as it is based on the full four-component DHF spinor wave functions and so spin–orbit coupling is included explicitly. The two small components are actually neglected, since they have been shown to be unimportant.[7a] The approach of Kahn, Hay, and Cowan[5] has the advantage of using single-component wave functions so that standard ab initio SCF codes can be used, which makes it simple to implement once the integrals over the ECPs have been calculated. Spin–orbit coupling is added in a subsequent diagonalization over a basis of LS coupled wave functions. The accuracy of this approach is limited by the size of the LS basis and by any approximations to the spin–orbit operator (see section III). So far the two approaches to relativistic ECPs have given very similar results,[7b,10] which supports the approximations made by Kahn, Hay, and Cowan.[5] The latter method has also been tested on a wide variety of systems (Xe_2^+,[10] XeF,[10] AuH,[11] AuCl,[11] HgH,[11] $HgCl_2$,[12] HgBr,[12] $HgCl$[12] and $Re_2Cl_8^{2-}$)[13] with basically good results compared to experiment. (See ref 5 for a discussion of additional approaches to relativistic ECPs.)

These studies have shown the incorporation of relativistic effects to be crucial in making reliable predictions of molecular properties. The calculated bond length (1.52 Å) in AuH, for example, is extremely close to the experimental bond length (1.5237 Å) when a *relativistic* ECP is used to replace the core orbitals of the Au atom.[11] By contrast, the use of a *nonrelativistic* potential for Au leads to a calculated bond length (1.81 Å) nearly 0.3 Å *longer* than the experimental value! Errors of 2–3 eV are introduced into excitation and ionization energies by neglecting relativistic effects, and these effects also play a large role in determining molecular charge densities, dipole moments, and transition moments. These manifestations can be readily understood from the relativistic contraction or expansion of the atomic orbitals involved in the molecular orbitals (cf. ref 11). Similar results have been found in Au_2 by Lee, Ermler, and Pitzer.[7c,d]

Returning to the subject of inorganic photochemistry we omitted one topic which is probably receiving more scrutiny than all the others combined, namely, laser isotope separation of uranium. The photodissociation of UF_6 to produce a reactive intermediate, UF_5, has many parallels with, say, the production of $Cr(CO)_5$ from photolysis of $Cr(CO)_6$. Thus, by studying the electronic structure of UF_5, we can begin to ascertain the differences between reactive metal complexes involving transition metals and actinides. The hope is that actinide or lanthanide photochemistry will provide new or better catalysts for chemical synthesis or improved ways of transforming solar energy into chemical or electrical energy.

We report here ab initio quality calculations using relativistic ECPs on UF_5. The calculations are used to investigate the geometry of UF_5, i.e., whether it is a square pyramid (C_{4v}) or a trigonal bipyramid (D_{3h}). The bonding in the ground state as well as the nature of the low-lying excited states are considered and compared to the results for UF_6.[14]

0002-7863/79/1501-5198$01.00/0

II. Qualitative Model for UF_5

Before we discuss the calculations in detail, a few qualitative remarks about the electronic structure of UF_5 are in order. The simplest model for the electronic structure of UF_5 is to assume that each electronegative fluorine extracts an electron from the uranium leading to a nominal $U^{5+}F_5^-$ structure. The electronic configuration of U^{5+} is $[Rn]5f^1$, so one expects a singly occupied 5f orbital on the uranium in UF_5. Since the 5f orbital is tight and basically nonbonding, the geometry of $U^{5+}F_5^-$ should be determined by minimizing the F^-–F^- Coulomb repulsions. There are two standard geometries for pentacoordinate complexes: square pyramidal (C_{4v}) and trigonal bipyramidal (D_{3h}). There is some flexibility in the square pyramidal structure, namely, the axial–equatorial F–U–F angle. Optimization of this angle to minimize the Coulomb repulsion leads to 104°. Comparing the optimal C_{4v} geometry with D_{3h}, one finds that the D_{3h} structure is slightly favored. Assuming a UF bond distance equal to that in UF_6 (2.00 Å), the D_{3h} structure is calculated to be 1.5 kcal/mol lower than the C_{4v}. Thus, the simple ionic model predicts the two structures to be very close in energy.

One can go beyond the above electrostatic arguments to consider the effect of the singly occupied 5f orbital. In D_{3h} and C_{4v} the sevenfold degenerate 5f orbital splits into five orbitals, two of which are doubly degenerate. Using simple ligand field theory the orbitals may be ordered by energy as follows: $e'' < a_2' < a_1' < e' < a_2''$ in D_{3h} and $b_2 < e < b_1 < a_1 < e$ in C_{4v}, as shown in the orbital correlation diagram in Figure 1. Therefore, the ground state for D_{3h} is predicted to be $^2E''$ and for C_{4v} to be $^2B_2$. The $^2E''$ state will, however, undergo a Jahn–Teller distortion[15] to lower symmetry (C_{2v}) to give a $^2A_2$ state (cf. Figure 1), so that the simple ionic model actually predicts a C_{4v} equilibrium geometry for UF_5. The above discussion must be tempered with the fact that the substantial effect of spin–orbit coupling on the uranium 5f orbital has been neglected.

Turning to the electronic spectrum of UF_5, one expects a series of very low-lying f → f transitions. These transitions should be weak as they correspond to forbidden transitions in the uranium atom. The next set of electronic transitions will be charge transfer from the fluorines to the uranium 5f orbitals. These are directly analogous to those in UF_6 and so should set in around 3 eV.[16,17]

III. Calculational Details

The calculational techniques employed for UF_5 are the same as those used for UF_6.[14] Since the basis sets, ECPs wave functions, and spin–orbit calculations are discussed in detail in the UF_6 paper, only a brief outline will be presented here.

The ECPs are obtained in four basic steps. (1) Numerical atomic wave functions are determined with either the nonrelativistic Hartree–Fock program of Froese-Fischer[18] for the lighter atoms or the relativistic Hartree–Fock program of Cowan and Griffin[9] for heavier atoms. In the relativistic calculation the Darwin and mass-velocity terms are added to the Hamiltonian. These terms lead to the major changes in the sizes and energies of the orbitals induced by relativistic effects. Spin–orbit coupling is added later in a separate calculation so one is still dealing with a simple one-component LS wave function. (2) The valence Hartree–Fock orbitals are transformed into smooth, nodeless pseudoorbitals by mixing in appropriate amounts of the core. (3) The pseudoorbitals are then inverted to give a numerical ECP using the equation

$$(t + U_l + \tilde{V}_{val})\tilde{\phi}_l = \epsilon_l\tilde{\phi}_l$$

where ϵ_l is the Hartree–Fock orbital energy, $\tilde{\phi}_l$ is the pseudoorbital, t is the kinetic energy operator, $\tilde{V}_{val}$ is the Coulomb and exchange operator for the valence orbitals, which will not be replaced, and U_l is the ECP for angular momentum l. (4)

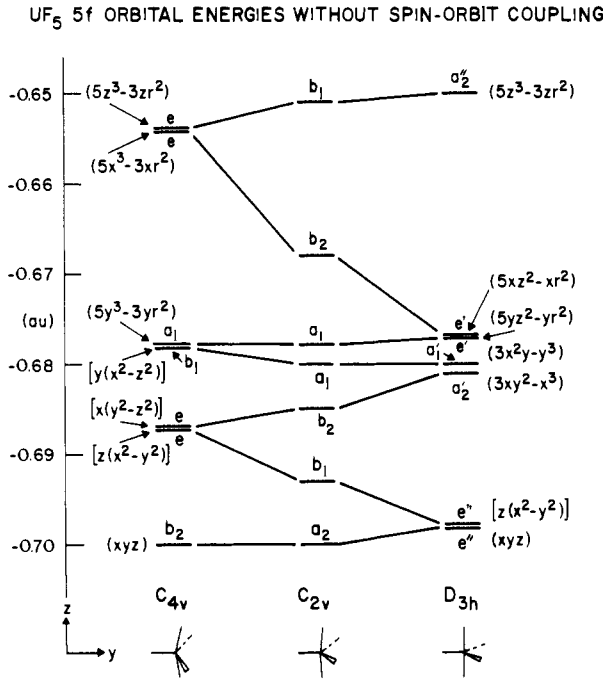

Figure 1. UF_5 5f orbital energies without spin–orbit coupling for C_{4v}, C_{2v}, and D_{3h} geometries.

The numerical ECPs are fit by nonlinear least-squares with Gaussians $r^n e^{-\alpha r^2}$ (n = 0, 1, 2). The total potential is a sum over the various angular momenta, so that for uranium we have

$$U(r) = U_g(r) + U_{s\text{-}g}(r)|s\rangle\langle s| + U_{p\text{-}g}(r)|p\rangle\langle p| + U_{d\text{-}g}(r)|d\rangle\langle d| + U_{f\text{-}g}|f\rangle\langle f|$$

where the maximum angular momentum is one greater than that in the core.

A relativistic ECP derived from U^{3+} atomic wave functions was used for uranium. Relativistic ECPs have also been derived from U^0 and U^{5+} atomic wave functions and tested on UF_6. The results were found to be surprisingly insensitive to the ECP.[14] Since the Mulliken population analysis indicated a charge of +2.4 on the uranium in UF_6, the ECP derived from U^{3+} was deemed most appropriate. As we shall see below, the charge on the uranium is basically unchanged in UF_5, i.e., +2.4, and so the U^{3+} potential is again appropriate. The uranium ECP replaces the effect of 78 electrons, i.e., the 6s and 6p electrons are treated explicitly. Normally, one would consider these as core electrons. For example, the electronic configuration of U^{3+} is . . . $6s^26p^65f^3$ and the 5f orbital energy is −1.1 hartrees compared to −1.9 hartrees for 6p and −2.9 hartrees for 6s. However, when one considers the spatial extent of these orbitals, one finds that the 6p orbital is significantly larger than the 5f, while the 6s and 5f are comparable in size. A nonrelativistic ECP was used to replace the 1s electrons on fluorine[14] so that UF_5 is reduced from a 137-electron to a 49-electron problem.

A double ζ quality basis was used with (4s4p3d4f) primitives contracted to [3s3p2d2f] on the uranium and (4s5p) contracted to [2s2p] on the fluorine.[14] The integrals were calculated using a new version of the BIGGMOLI program of Raffenetti[19] extended to f functions. The integral times ranged from 10 to 48 min with the latter value corresponding to a C_s geometry. All two-electron integrals with absolute values $\geq 10^{-7}$ au were retained in the SCF calculations, which led to approximately 4×10^6 integrals.

All the calculations on the ground state of UF_5 were open-shell restricted Hartree–Fock calculations,[20] which required

Table I. Optimum Geometries for the Ground State of UF_5 without Spin-Orbit Coupling (Distances in Å)

	$R(UF_{ax})$	$R(UF_{eq})$	$\angle F_{ax}UF_{eq}$, deg
C_{4v}	2.00	2.00	100
D_{3h}	1.99	2.02	90[a]

[a] Determined by symmetry.

from 27 to 52 s per iteration depending on the molecular symmetry. The geometry optimization for C_{4v} and D_{3h} involved independent variation of each degree of freedom (three for C_{4v} and two for D_{3h}) with simple three-point parabolic fits. Increments of $0.25a_0$ and 10° were employed for the bond lengths and bond angles, respectively.

The energies of the low-lying f → f transitions were calculated using the improved virtual orbital (IVO) method.[21] Although the core electrons are not allowed to relax, the one-electron IVO excitation energies are expected to be relatively accurate, since the 5f orbitals are basically nonbonding.

Spin-orbit mixing of the low-lying states associated with the unpaired electron in the seven 5f orbitals was performed using an effective one-electron, one-center spin-orbit operator[14,22]

$$\hat{H}_{S\text{-}O} = \sum_{A,i} \sum_{l=1} |l\rangle \frac{Z_{lA}^{\text{eff}}}{r_{iA}^{3}} (l_A \cdot s_i) \langle l|$$

where Z_{lA}^{eff} denotes the effective nuclear charge of center A for basis functions having orbital angular momentum l. The Z_{lA}^{eff} are chosen to reproduce the atomic spin-orbit parameters.[23] For fluorine the experimental splitting is used for the 2p orbital,[24] while for uranium the theoretical values determined from the numerical atomic wave functions with the Blume-Watson method[25] are used for the 5f, 6d, and 6p orbitals.[14] For UF_5 the spin-orbit mixing reduces to a one-electron problem. The spin-orbit interaction matrix is evaluated over the singly occupied orbitals determined by the IVO calculation (including the ground state 5f orbital) and added to the diagonal orbital energies. The resulting matrix is then diagonalized to determine the new spin-orbit states.

IV. Results

Optimization of the C_{4v} geometry (without spin-orbit coupling) gives an axial-equatorial FUF angle of 100° and equal axial and equatorial UF bond lengths of 2.00 Å. The latter are the same as the bond length in UF_6.[26] Optimization of the D_{3h} geometry also leads to axial and equatorial UF bond lengths very close to that in UF_6. Specifically, the axial UF distance is calculated to be 1.99 Å, while the equatorial distance is 2.02 Å. However, the energy difference between the optimum geometry and a geometry with all bond lengths equal to 2.00 Å is only 6×10^{-5} au! Given the flatness of the surface the calculated bond lengths are expected to be accurate to only ±0.04 Å. Therefore, for convenience and without loss of accuracy, any future reference to the optimum D_{3h} geometry will actually refer to the geometry with equal bond lengths of 2.00 Å. The results of the geometry optimization are summarized in Table I.

As predicted by ligand field theory the ground state of UF_5 is $^2B_2$ for the square pyramidal geometry and $^2E''$ for the trigonal bipyramid. The energy of the $^2B_2$ state is calculated to be 1.1 kcal/mol lower than that of the $^2E''$. Since the $^2E''$ will undergo a Jahn-Teller distortion, we considered the C_{2v} path connecting the D_{3h} and C_{4v} structures (cf. Figure 1). The C_{2v} path is determined by first selecting one of the three equatorial fluorines in the D_{3h} structure to become the axial fluorine (F_{ea}) in the C_{4v} structure. The other two D_{3h} equatorial fluorines (F_{ee}) remain equatorial in C_{4v}, while the two D_{3h} axial fluorines (F_{ae}) become equatorial in C_{4v}. Thus the C_{2v} pathway connecting D_{3h} with C_{4v} is described by a decrease in the F_{ea}-U-F_{ee} angle from 120 to 100° and an increase in the F_{ea}-U-F_{ae} angle from 90 to 100°. The energies along this path are tabulated in Table II. We see that the energy decreases monotonically from D_{3h} to C_{4v}, so that without spin-orbit coupling UF_5 is predicted to have a square pyramidal geometry.

Table II. Total Energies for the C_{2v} Path Connecting the D_{3h} and C_{4v} Structures of UF_5[a]

sym-metry	$\angle F_{ea}$-U-F_{ee}, deg	$\angle F_{ea}$-U-F_{ae}, deg	without spin-orbit ΔE	with spin-orbit ΔE
C_{4v}	100	100	0.0[b]	−7.4
C_{2v}	102	98	0.0	
C_{2v}	110	95	0.2	−7.7
C_{2v}	118	92	0.8	
D_{3h}	120	90	1.1	−8.3
C_{2v}	122	88	1.8	

[a] All UF bond lengths are equal to 2.00 Å. The energies are in kcal/mol. [b] Absolute total energy is −173.590 73 hartrees.

As discussed in the previous section introduction of spin-orbit coupling reduces to a one-electron problem for UF_5. Figure 1 gives the calculated 5f orbital energies for the C_{4v} and D_{3h} geometries as well as for the C_{2v} geometry midway between them. Using these orbital energies and the calculated spin-orbit interactions among the 5f orbitals in UF_5, a new set of spin-orbit energies was determined, presented schematically in Figure 2. (A discussion of the double group symmetries will be presented in the next section.) In all cases spin-orbit coupling significantly lowered the energy of the UF_5 ground state, by 7.4, 7.9, and 9.4 kcal/mol for the C_{4v}, C_{2v}, and D_{3h} structures, respectively (see Figure 3 and Table II). The trigonal bipyramid is now 1 kcal/mol lower than the square pyramid. The double group symmetry of the ground state in D'_{3h} is Γ_9 and Γ_7 in C'_{4v}. More important, the Γ_9 state is *not* subject to a Jahn-Teller distortion, since it is a simple Kramers' doublet[27] (i.e., twofold degenerate as opposed to the fourfold degenerate $^2E''$ state). Therefore, the calculations with spin-orbit coupling predict the equilibrium geometry of UF_5 to be trigonal bipyramid.

Table III gives the calculated excitation energies and wavelengths for the f-f transitions in UF_5 including spin-orbit effects. All the transitions are dipole allowed and the oscillator strengths for *all* the possible transitions among the 5f orbitals are given in Table IV for both D_{3h} and C_{4v} geometries. Although the transitions are dipole allowed, they are very weak with oscillator strengths less than 10^{-4}.

V. Discussion

One of the major goals of these calculations on UF_5 was to determine its equilibrium geometry. The major result, however, is that UF_5 is fluxional, i.e., if UF_5 possesses any appreciable internal energy it will not have a well-defined geometry. The calculations including spin-orbit coupling predict the energies of the D_{3h} and C_{4v} geometries to be separated by less than 1 kcal/mol. More important, the C_{2v} pathway connecting the two structures is monotonic, and hence the molecule can pass readily and rapidly from one geometry to another. All five fluorines can thus be continually interchanged along these routes. A few C_s pathways were considered and small barriers (~5 kcal/mol) were encountered. The calculations indicate that the trigonal bipyramid is slightly lower in energy, but the energy separation is so small that the results are simply not accurate enough to predict with any confidence which structure is actually lower in energy. On the other hand, the calculations are accurate enough to place confidence in the prediction of fluxional behavior for UF_5.

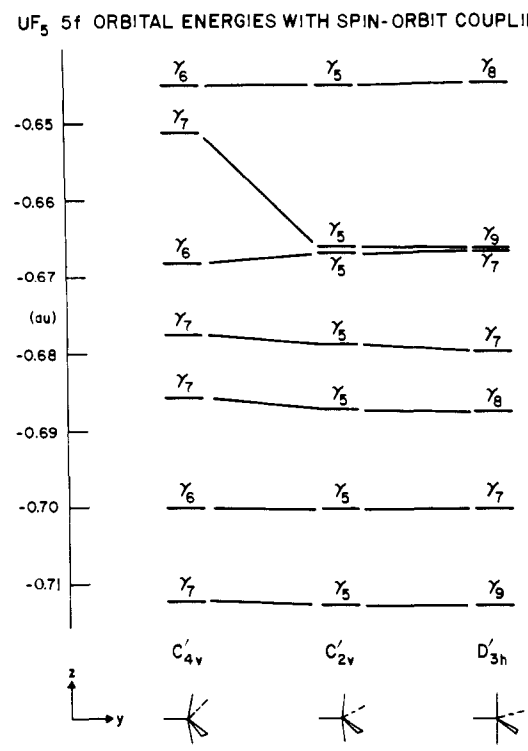

Figure 2. UF_5 5f orbital energies with spin-orbit coupling for C'_{4v}, C'_{2v}, and D'_{3h} geometries.

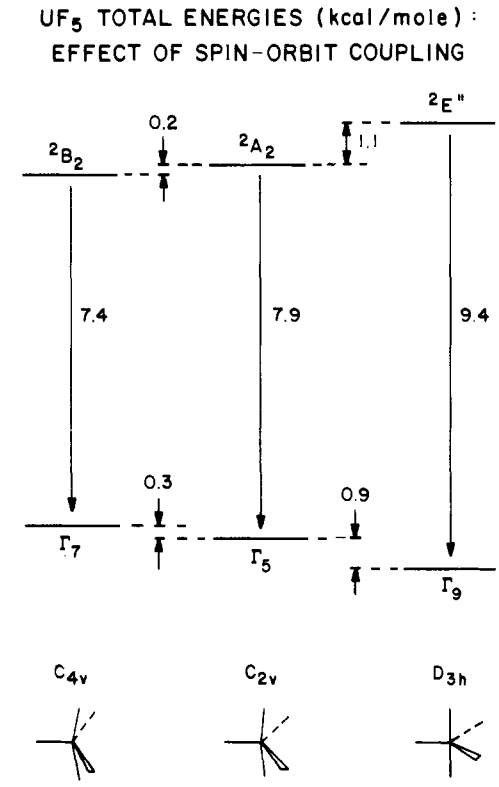

Figure 3. UF_5 total energies with and without spin-orbit coupling for C_{4v}, C_{2v}, and D_{3h} geometries.

Table III. Calculated f–f Transition Energies ($\times 10^3$ cm^{-1}) and Wavelengths (μm) for D'_{3h} and C'_{4v} Geometries of UF_5 Including Spin–Orbit Coupling

D'_{3h}			C'_{4v}		
	ΔE	λ		ΔE	λ
$1\Gamma_9 \rightarrow 1\Gamma_7$	2.0	4.90	$1\Gamma_7 \rightarrow 1\Gamma_6$	2.7	3.67
$1\Gamma_9 \rightarrow 1\Gamma_8$	5.5	1.82	$1\Gamma_7 \rightarrow 2\Gamma_7$	5.7	1.75
$1\Gamma_9 \rightarrow 2\Gamma_7$	7.3	1.37	$1\Gamma_7 \rightarrow 3\Gamma_7$	7.6	1.31
$1\Gamma_9 \rightarrow 3\Gamma_7$	10.1	0.991	$1\Gamma_7 \rightarrow 2\Gamma_6$	9.6	1.04
$1\Gamma_9 \rightarrow 2\Gamma_9$	10.1	0.987	$1\Gamma_7 \rightarrow 4\Gamma_7$	13.3	0.753
$1\Gamma_9 \rightarrow 2\Gamma_8$	15.0	0.666	$1\Gamma_7 \rightarrow 3\Gamma_6$	14.6	0.683

Table IV. Calculated Dipole Oscillator Strengths for All the Transitions among the 5f Orbitals in UF_5 Including Spin–Orbit Coupling for the D'_{3h} and C'_{4v} Geometries[a]

D'_{3h}						
	$1\Gamma_9$	$1\Gamma_7$	$1\Gamma_8$	$2\Gamma_7$	$3\Gamma_9$	$2\Gamma_9$
$1\Gamma_7$	1.28(−5)					
$1\Gamma_8$	1.35(−7)	7.32(−6)				
$2\Gamma_7$	1.84(−6)	0.	1.17(−6)			
$3\Gamma_7$	1.29(−6)	0.	1.00(−4)	0.		
$2\Gamma_9$	8.65(−8)	8.33(−5)	8.20(−7)	3.21(−5)	3.91(−8)	
$2\Gamma_8$	8.43(−6)	7.47(−5)	0.	3.21(−5)	6.47(−5)	8.78(−8)

C'_{4v}						
	$1\Gamma_7$	$1\Gamma_6$	$2\Gamma_7$	$3\Gamma_7$	$2\Gamma_6$	4Γ
$1\Gamma_6$	5.86(−6)					
$2\Gamma_7$	2.60(−5)	1.10(−5)				
$3\Gamma_7$	1.93(−5)	1.19(−5)	9.26(−6)			
$2\Gamma_6$	2.03(−5)	3.57(−5)	7.44(−6)	5.95(−6)		
$4\Gamma_7$	2.55(−5)	2.60(−5)	3.93(−5)	2.88(−5)	5.92(−6)	
$3\Gamma_6$	2.12(−5)	1.47(−5)	3.45(−5)	1.76(−5)	1.11(−5)	6.84(−6)

[a] Note: 2.18(−7) = 2.18×10^{-7}.

Table V. Mulliken Population Analysis for the D_{3h} and C_{4v} Geometries of UF_5 and for UF_6

	fluorine				uranium			
	equatorial		axial					
	s	p	s	p	s	p	d	f
UF_5 (D_{3h})	1.93	5.55	1.94	5.53	2.18	6.30	1.20	1.94
UF_5 (C_{4v})	1.94	5.54	1.94	5.54	2.18	6.31	1.18	1.97
UF_6 (O_h)[a]	1.94	5.45	1.94	5.45	2.21	6.36	1.38	1.67

[a] Reference 14.

There are four aspects or ramifications of the fluxional behavior of UF_5, which warrant further discussion: (1) the nature of the bonding in UF_5, (2) the effect of spin-orbit coupling, (3) the photogeneration of UF_5, and (4) the effect of the environment on the geometry of UF_5.

A. Bonding in UF_5. The ionic model of UF_5 discussed earlier would predict Mulliken populations of 8 for the fluorines ($2s^22p^6$) and 9 for uranium ($6s^26p^65f^1$). The calculated Mulliken populations for the C_{4v} and D_{3h} structures of UF_5 are given in Table V along with those for UF_6.[14] The charge distributions for the two UF_5 geometry differ negligibly. Moreover, the populations for the equatorial and axial fluorines are nearly indistinguishable, which is consistent with the negligible difference in U–F bond lengths. As expected, the simple ionic model overestimates the charge transfer from uranium to the fluorines. The actual charge on the uranium is +2.4 instead of +5 as predicted by the ionic model. The reduced charge may be viewed as arising from back-donation or back-bonding from the fluorines into the uranium orbitals. The use of the term back-bonding, of course, arises only because we have selected the simple ionic model as our zero-order reference for describing the bonding in UF_5. However, the fact that the Mulliken populations for the p and d orbitals exceed those for ground-state neutral uranium atom ($6s^26p^65f^36d^17s^2$) seems to give some validity to the idea of back-bonding.

Continuing with the above line of argument the s and p Mulliken populations on the uranium may be divided, albeit arbitrarily, into a nonbonding part $6s^26p^6$ and back-bonding

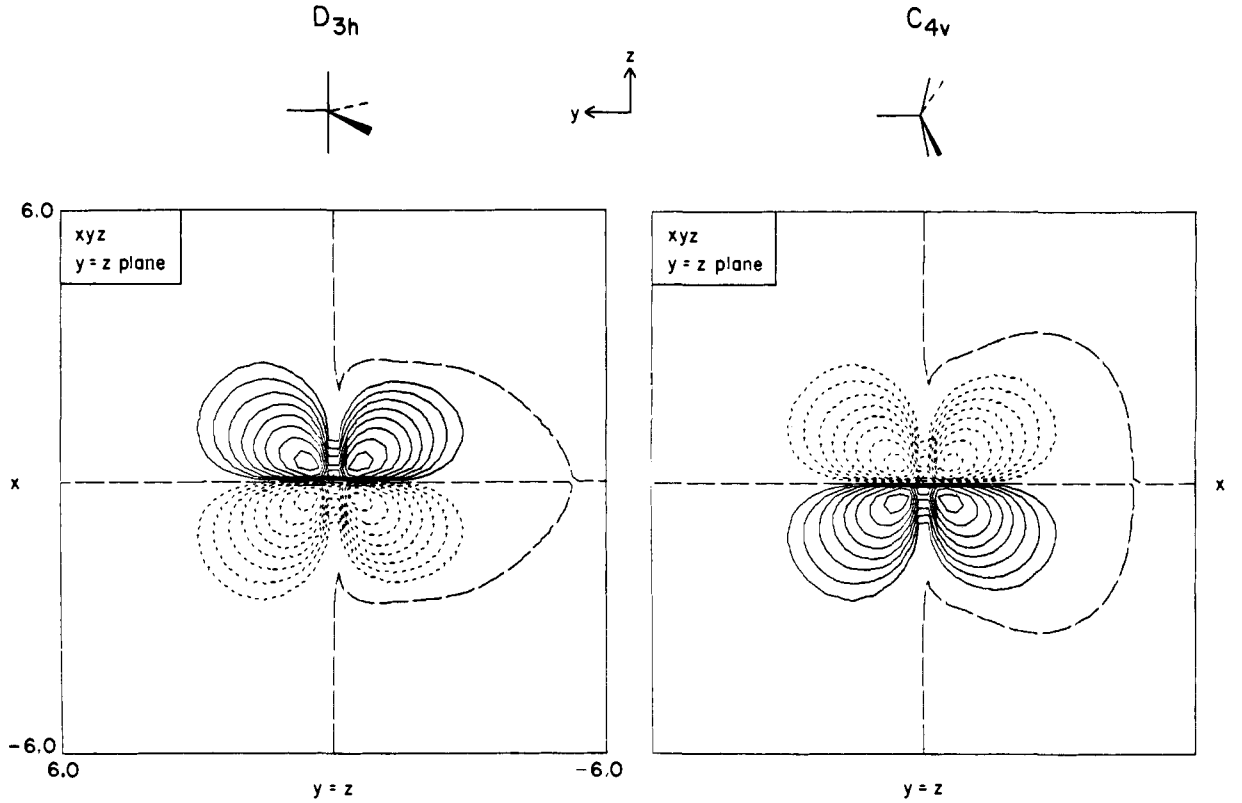

Figure 4. Contour plots of f_{xyz} orbital for D_{3h} and C_{4v} geometries. Contours are spaced logarithmically starting at 0.02 and increasing by a factor of 1.584 89 ($=10^{0.2}$).

into the 7s and 7p orbitals of 0.2 and 0.3, respectively. Similarly the f Mulliken population is partitioned into the singly occupied $5f_{xyz}$ and 0.9 of back-bonding into the other 5f orbitals. Thus, the back-bonding is greatest into the 6d orbitals. One point about the fluorines is worth mentioning, namely, the Mulliken population for the fluorine 2p orbital pointed toward the uranium is 1.76–1.77 compared to 1.89–1.90 for the 2p orbitals perpendicular to the UF axis.

Comparing the Mulliken populations for UF_5 to those for UF_6 a number of interesting points become apparent. First, the overall charge on the uranium is unchanged, namely, +2.4. This was not unexpected, since calculations on UF_6^- [14] and the excited states of UF_6,[17] involving charge transfer from a fluorine orbital to a uranium 5f orbital, showed only negligible changes in the charge on the uranium. In all cases, direct occupation of a uranium 5f orbital leads to redistribution of the other electrons so as to maintain the same charge on the uranium. In the case of UF_5 (relative to ground-state UF_6) the redistribution corresponds to a diminishing of the back-bonding into the s, p, d, and f orbitals. The change is largest for the 5f orbitals, where the back-bonding decreases from 1.7 electrons in UF_6 to 0.9 in UF_5.

It is clear from the above discussion that the bonding in UF_5 and UF_6 is similar, i.e., basically ionic with significant back-bonding into the uranium 6d and 5f orbitals. The excellent predictions of the simple ionic model as to the F_{ax}–U–F_{eq} angle in the C_{4v} structure and the near degeneracy of the C_{4v} and D_{3h} structure are not surprising given that the actual charge on uranium is +2.4.

B. Excited 5f Orbitals. Since this is one of the first ab initio molecular calculations involving f orbitals, it seems appropriate to digress for a moment to discuss in more detail the nature of the singly occupied 5f orbitals in the ground and low-lying excited states of UF_5. The 5f orbital energies are shown in Figure 1 for the C_{4v}, C_{2v}, and D_{3h} geometries. To obtain a better feel of the changes of the 5f orbitals induced by the movement of the fluorines we have made contour plots of the orbitals for the C_{4v} and D_{3h} structures.

Figure 4 compares the f_{xyz} orbital in C_{4v} and D_{3h}. The f_{xyz} orbital is elusive, since it vanishes in the normal plotting planes, i.e., $x = 0$, $y = 0$, and $z = 0$. Therefore, we have plotted it in the $y = z$ plane. As can be seen the f_{xyz} orbital does not change significantly. Superimposing the two contour plots reveals that the lobes for $y > 0$ constrict slightly as one goes from C_{4v} to D_{3h}. Hence, the kinetic energy of the f_{xyz} orbital should be larger in D_{3h}, which is confirmed by the higher orbital energy (cf. Figure 1).

From Figure 1, the lowest excited 5f orbital in C_{4v} is a doubly degenerate e, which splits into e″ and a_2' in D_{3h}. Figure 5 presents contour plots of the e, e″, and a_2' orbitals. The positions of the fluorines are easily discerned from the 2p orbital contours. The $f_{z(y^2-z^2)}$ component of the e orbital is plotted in the xy plane. Comparing the e and e″ orbitals, we see that the $f_{z(x^2-y^2)}$ orbital is stabilized as the number of nodal planes is reduced. Note also the similarity between the degenerate e″ orbitals (f_{xyz} and $f_{z(x^2-y^2)}$) in D_{3h}. The other component of the e orbital, $f_{x(y^2-z^2)}$, is destabilized as the nodal patterns become more pronounced. The orbital changes character from $f_{x(y^2-z^2)}$ to $f_{3xy^2-x^3}$. The latter orbital has a striking threefold axis of symmetry, since $3xy^2 - x^3 = r^3 \cos 3\theta$.

The changes become more complex when one considers the nearly degenerate $b_1(f_{y(x^2-z^2)})$ and $a_1(f_{5y^3-3yr^2})$ orbitals in C_{4v}. The two orbitals mix and correlate with the $a_1'(f_{3x^2y-y^3})$ and $e_y'(f_{5yz^2-yr^2})$ orbitals in D_{3h}. Figure 6 gives plots of the a_1 and b_1 orbitals in the yz plane as well as plots of the a_1' and e_y' orbitals in the yz and xy planes. The plots of the a_1 and b_1 orbitals in the yz plane are equivalent to those in the xy plane except that the b_1 orbital changes sign and we denote this by the "$-xy$" plane in Figure 6. A little algebra shows that the mixing of the C_{4v} orbitals in D_{3h} is $a_1' = \frac{3}{2}\, b_1 - \frac{1}{2}\, a_1$ and $e_y' = -\frac{5}{2}\, b_1 - \frac{1}{2}\, a_1$. Using these expressions one can see by adding and subtracting the a_1 and b_1 orbitals how they mix to

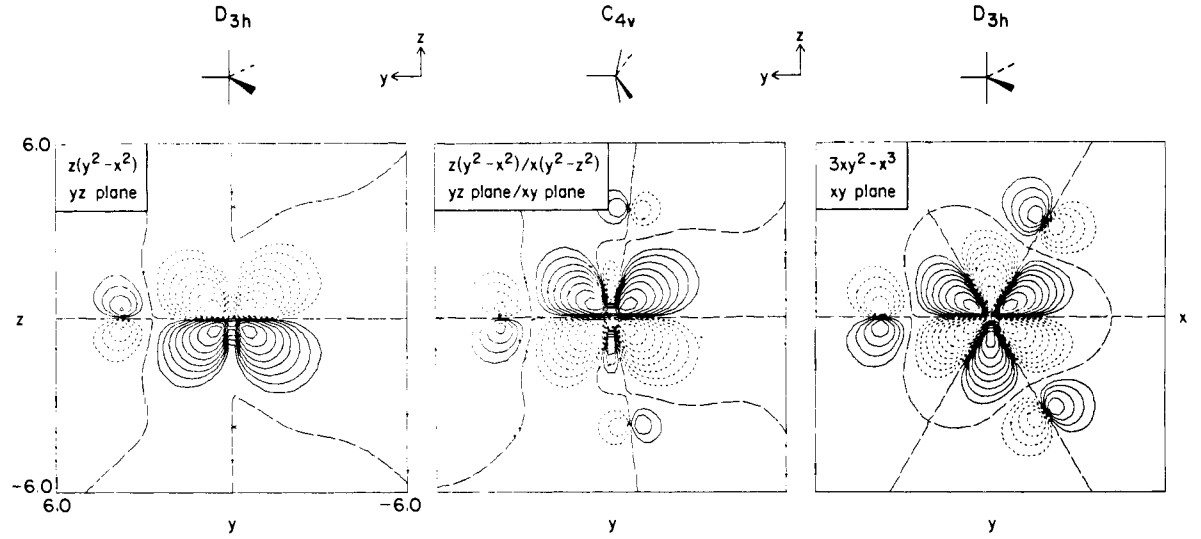

Figure 5. Contour plots of $f_{z(y^2-x^2)}/f_{x(y^2-z^2)}$ in C_{4v} and $f_{z(y^2-x^2)}$ and f_{3xy-x^3} in D_{3h}.

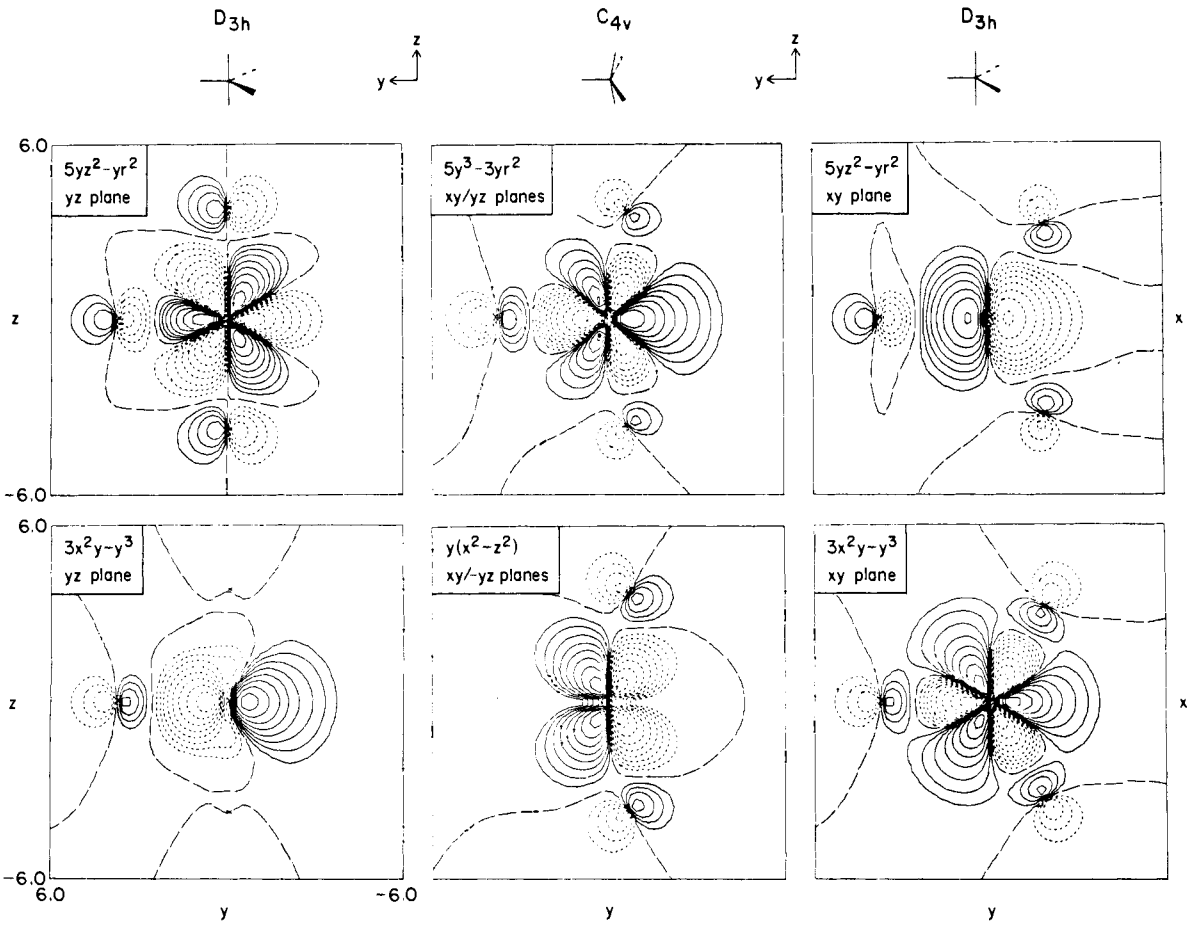

Figure 6. Contour plots of $f_{5y^3-3yr^2}$ and $f_{y(x^2-z^2)}$ in C_{4v} and $f_{5yz^2-yr^2}$ and $f_{3x^2y-y^3}$ in D_{3h}.

give the a_1' and e_y' orbitals. The overall energies change only slightly in going from C_{4v} to D_{3h}. Again the a_1' orbital has an obvious threefold symmetry, since $3x^2y - y^3 = r^3 \sin 3\theta$.

The final pair of C_{4v} orbitals is degenerate ($f_{5z^3-3zr^2}$, $f_{5x^3-3xr^2}$). The $e_z(f_{5z^3-3zr^2})$ goes over directly to the a_2'' orbital in D_{3h}. Figure 8 shows contour plots of the e_z and a_2'' orbitals. The $f_{5z^3-3zr^2}$ is clearly destabilized as the fluorines are moved onto the z axis. The increase in orbital energy is shown in Figure 1. The other component of the e orbital ($f_{5x^3-3xr^2}$) is greatly stabilized in D_{3h}. The $f_{5x^3-3xr^2}$ ($2e_x$) and $f_{x(y^2-z^2)}$ ($1e_x$) orbitals mix in D_{3h} to give the a_2' and e_x' orbitals according to $a_2' = \frac{3}{2}(1e_x) - \frac{1}{2}(2e_x)$ and $e_x' = -\frac{5}{2}(1e_x) - \frac{1}{2}(2e_x)$. Comparing the plots of $2e_z$ in Figure 7 (which is the same as that for $2e_x$ in the xy plane) and of $1e_z$ in Figure 5 (which is the same as that for $1e_x$ in the xy plane), one sees that adding and subtracting the orbitals gives the a_2' orbital in Figure 5 and an e_x' orbital ($f_{5xz^2-xr^2}$), which would look like the e_y' orbital ($f_{5yz^2-yr^2}$) in Figure 6, rotated 90°. It is evident from Figure 7 that moving the fluorines away from the z axis stabilizes the $f_{5x^3-3xr^2}$ orbital as shown in Figure 1.

C. Effect of Spin-Orbit Coupling. The effect of spin-orbit coupling on the geometry of UF_5 is very interesting. Without

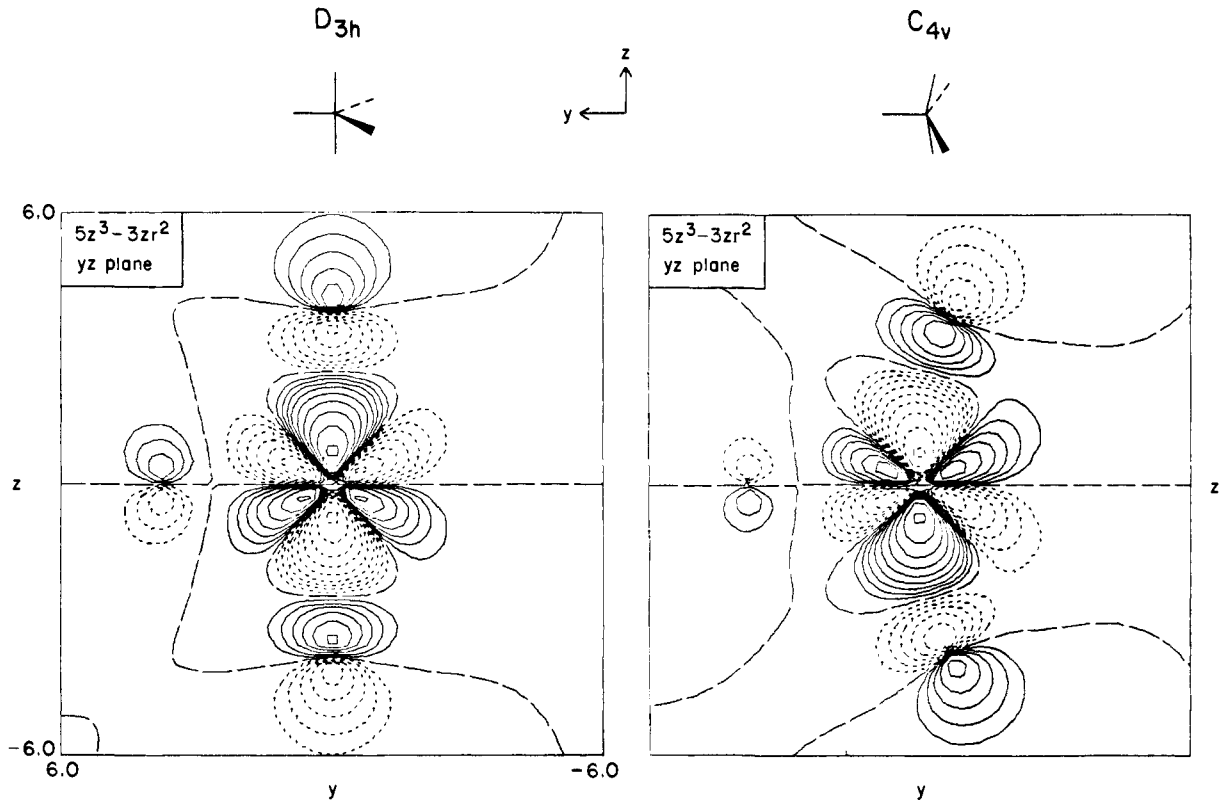

Figure 7. Contour plots of $f_{5z^2-3r^2}$ orbital in D_{3h} and C_{4v}.

spin-orbit coupling the square pyramidal geometry is actually lower than the trigonal bipyramid. Moreover, the ground state in C_{4v} is $^2B_2$, which corresponds to occupation of the f_{xyz} orbital. As the C_{4v} geometry is deformed into D_{3h} symmetry, the f_{xyz} orbital is destabilized and becomes degenerate with the $f_{z(x^2-y^2)}$ orbital (cf. Figure 1), so the ground state is now $^2E''$. The Jahn-Teller theorem[15] tells us what we already know, namely, that the $^2E''$ state is subject to a nuclear distortion that will lower the energy. The distortion is, of course, the C_{2v} pathway connecting the D_{3h} and C_{4v} structures. Note also that the other component ($^2B_1$) of the $^2E''$ state is destabilized along this path as expected from the Jahn-Teller theorem (cf. Figure 1). Finally, the $^2B_1$ state ($f_{z(x^2-y^2)}$) actually becomes the ground state, if one follows the C_{2v} pathway in the opposite direction (i.e., starting from D_{3h} and moving away from C_{4v}).

Spin-orbit coupling mixes the 5f orbitals among one another. The size of the spin-orbit interaction may be discerned from the spin-orbit coupling constant for the 5f orbitals in uranium atom, ζ_{5f} = 1879 cm^{-1} = 0.009 hartree.[14] From Figure 1, the ligand field splitting for the 5f orbitals is 0.047 hartree, so that the spin-orbit will be significant compared to the ligand field, but will not dominate it.

Inclusion of spin-orbit coupling means that the symmetry of the electron spin must be included when determining the symmetry of the wave function. Since the electron has angular momentum of $^1/_2$, a rotation through 2π does not leave it unchanged, but rather reverses its sign. As a result, one must use double groups. The reader is referred to the excellent elementary introduction to double groups of Cotton[28] and to Koster et al.[29] for the double group character tables for C'_{2v}, C'_{4v}, and D'_{3h}.

The electron spin transforms as γ_5 in C'_{2v}, γ_6 in C'_{4v}, and γ_7 in D'_{3h}. Since the direct product in C'_{2v} of γ_5 with any of the spatial symmetries gives γ_5, all seven 5f orbitals in UF_5 transform as γ_5, as indicated in Figure 2. Consequently in C'_{2v} symmetry all the 5f orbitals can mix with one another. For C'_{4v} and D'_{3h} the direct products of the space and spin parts of the 5f orbitals are shown in Table VI. The resultant spin-orbitals transform in C'_{4v} as either γ_6 or γ_7. The γ_6 orbitals will be mixtures of all the 5f orbitals except f_{xyz} and $f_{y(x^2-z^2)}$, while the γ_7 orbitals are mixtures of all the orbitals except $f_{5y^3-3yr^2}$. Finally, in D'_{3h} the 5f spin-orbits transform as γ_7, γ_8, or γ_9. The γ_7 orbitals are mixtures of f_{xyz}, $f_{z(x^2-y^2)}$, $f_{3xy^2-x^3}$, and $f_{3x^2y-y^3}$, the γ_8 orbitals are mixtures of $f_{5yz^2-yr^2}$, $f_{5xz^2-xr^2}$, and $f_{5z^3-3zr^2}$, and the γ_9 orbitals are mixtures of f_{xyz}, $f_{z(x^2-y^2)}$, $f_{5yz^2-yr^2}$, and $f_{5xz^2-yr^2}$. For all the symmetries the 5f spin-orbitals are doubly degenerate arising from the α and β spin (the Kramers degeneracy).

Table VI. Double-Group 5f Spin-Orbital Symmetries for UF_5[a]

space			spin		total
		C'_{4v}			
f_{xyz}	$\gamma_4(b_2)$	⊗	γ_6	=	γ_7
$f_{z(x^2-y^2)}$, $f_{x(y^2-z^2)}$	$\gamma_5(e)$	⊗	γ_6	=	$\gamma_6 \oplus \gamma_7$
$f_{y(x^2-z^2)}$	$\gamma_3(b_1)$	⊗	γ_6	=	γ_7
$f_{5y^3-3yr^2}$	$\gamma_1(a_1)$	⊗	γ_6	=	γ_6
$f_{5x^3-3xr^2}$, $f_{5z^3-3zr^2}$	$\gamma_5(e)$	⊗	γ_6	=	$\gamma_6 \oplus \gamma_7$
		D'_{3h}			
f_{xyz}, $f_{z(x^2-y^2)}$	$\gamma_5(e'')$	⊗	γ_7	=	$\gamma_7 \oplus \gamma_9$
$f_{3xy^2-x^3}$	$\gamma_2(a'_2)$	⊗	γ_7	=	γ_7
$f_{3x^2y-y^3}$	$\gamma_1(a'_1)$	⊗	γ_7	=	γ_7
$f_{5yz^2-yr^2}$, $f_{5xz^2-xr^2}$	$\gamma_6(e')$	⊗	γ_7	=	$\gamma_8 \oplus \gamma_9$
$f_{5z^3-3zr^2}$	$\gamma_4(a''_2)$	⊗	γ_7	=	γ_8

[a] Note y is chosen as C_4 axis in C_{4v}.

Comparing Figures 1 and 2, spin-orbit coupling is seen to spread out the 5f orbital energies, removing all the degeneracies or near degeneracies, e.g., the a_1 and b_1 states in C_{4v}. In all cases the 5f orbital occupied in the ground state of UF_5 is significantly stabilized. The effect on the total energies for C_{4v},

Table VII. Direct Products for 5f Orbital Double Group Symmetries in UF_5[a]

C'_{4v}

$\gamma_6 \otimes \gamma_6 = \gamma_1(a_1) \oplus \gamma_2(a_2) \oplus \gamma_5(e)$
$\gamma_6 \otimes \gamma_7 = \gamma_3(b_1) \oplus \gamma_4(b_2) \oplus \gamma_5(e)$
$\gamma_7 \otimes \gamma_7 = \gamma_1(a_1) \oplus \gamma_2(a_2) \oplus \gamma_5(e)$
$y \sim \gamma_1(a_1)$; $(x,y) \sim \gamma_5(e)$

D'_{3h}

$\gamma_7 \otimes \gamma_7 = \gamma_1(a_1') \oplus \gamma_2(a_2') \oplus \gamma_5(e'')$
$\gamma_7 \otimes \gamma_8 = \gamma_3(a_1'') \oplus \gamma_4(a_2'') \oplus \gamma_6(e')$
$\gamma_7 \otimes \gamma_9 = \gamma_5(e'') \oplus \gamma_6(e')$
$\gamma_8 \otimes \gamma_8 = \gamma_1(a_1') \oplus \gamma_2(a_2') \oplus \gamma_5(e'')$
$\gamma_8 \otimes \gamma_9 = \gamma_5(e'') \oplus \gamma_6(e')$
$\gamma_9 \otimes \gamma_9 = \gamma_1(a_1') \oplus \gamma_2(a_2') \oplus \gamma_3(a_1'') \oplus \gamma_4(a_2'')$
$z \sim \gamma_4(a_2'')$; $(x,y) \sim \gamma_6(e')$

[a] Note y is chosen as C_4 axis in C_{4v}.

C_{2v}, and D_{3h} is diagrammed in Figure 3. The larger stabilization for the trigonal bipyramid arises from the degenerate e″ orbital, which splits strongly with spin–orbit coupling.

The most interesting consequence of the spin–orbit interaction is that now the trigonal bipyramid is more stable than the square pyramid. In addition, the trigonal bipyramidal geometry is predicted to be the minimum energy geometry for UF_5, which was not possible without spin–orbit coupling because of the Jahn–Teller theorem. In this case, the spin–orbit interaction (~7–9 kcal/mol) dominates the Jahn–Teller forces (~1 kcal/mol). It should be noted that the pathway between the D'_{3h} and C'_{4v} structures remains monotonic via the C'_{2v} pathway and so UF_5 is still predicted to be fluxional.

In Table V, the calculated energies and wavelengths are given for the f–f transitions in UF_5. The analogous f–f transitions in uranium atom are, of course, dipole forbidden. Table VII gives the direct products for the 5f orbital symmetries in C'_{4v} and D'_{3h}. We see that in C'_{4v} *all* the f–f transitions are dipole allowed, while in D'_{3h} only the $\gamma_7 \rightarrow \gamma_7$ and $\gamma_8 \rightarrow \gamma_8$ transitions are dipole forbidden. Nevertheless, the forbidden origin in the f–f transitions is evident in the weak dipole transition moments and oscillator strengths (cf. Table IV). It is interesting to note that for C'_{4v}, where the 5f orbitals are more generally mixed than in D'_{3h}, the transition moments vary over a smaller range, 0.05–0.10 D, compared to 0.004–0.22 D for D'_{3h}. Only order-of-magnitude accuracy is expected for the calculated oscillator strengths given the simplicity of the IVO wave functions.[30] Additional errors arising from the use of relativistic ECPs are not expected to be significant. Previous calculations of electric dipole transition moments using relativistic ECPs have given good agreement with experiment.[7b,12] Moreover, the work of Hafner and Schwarz[31] on atomic transition probabilities using relativistic pseudopotential[32] shows that errors introduced by core-valence correlation effects are generally small.

It is appropriate at this point to compare our results to the other published calculations on UF_5. Maylotte, St. Peters, and Messmer[33] reported no relativistic Xα scattered-wave calculations on UF_5. Their calculations were performed at a C_{4v} geometry similar to our optimized geometry. They reported orbital energies and transition energies. Because they neglected relativistic effects, the ordering and spacing of their orbital energies are very different from ours. In addition, there are large errors in their excitation energies, as they find charge-transfer bands starting at 1 μm or 10×10^3 cm^{-1}, where our preliminary results[34] indicate that the charge-transfer bands ensue at 25×10^3 cm^{-1} or higher as in UF_6.[16,17] The large discrepancies between the calculations of Maylotte et al.[33] and the present work may be ascribed to their neglect of important relativistic effects and to deficiencies in the Xα scattered wave method.

Recently, Rosen and Fricke[35] have reported nonrelativistic Hartree–Fock–Slater and relativistic Dirac–Slater calculations on UF_5 assuming a C_{4v} geometry. The ordering of the 5f orbitals in the relativistic calculation agrees with our results. Their results[35] show that relativistic effects shift the charge-transfer bands to higher energy (~24×10^3 cm^{-1}) in good agreement with our preliminary results.[34] Rosen and Fricke[35] calculated wavelengths for four f–f transitions, namely, $1\Gamma_7 \rightarrow 1\Gamma_6$ (1.82 μm), $2\Gamma_7$ (1.29 μm), $4\Gamma_7$ (0.697 μm), and $3\Gamma_6$ (0.633 μm). Comparison with our results in Table III shows that our calculations predict considerably longer wavelengths for all the transitions. A similar discrepancy between IVO calculations using relativistic ECPs and local exchange calculations occurred for the f–f transitions in UF_6^-.[14] In that case experimental data are available and the IVO transition energies are too high by 0.1–0.2 eV, while the local exchange results are too high by 0.2–0.7 eV. Given the similarity of transitions under consideration in UF_5 and UF_6^-, we expect the present IVO calculations on UF_5 to be more accurate. One SCF calculation was performed on a 5f excited state of UF_5. The excitation energy decreased by 0.18 eV as the other electrons were allowed to adjust to the excitation. This relaxation energy is consistent with the errors observed in UF_6^-.[14]

D. Photogeneration of UF_5. Infrared spectroscopic studies of UF_5 have been performed both in inert matrices[36-38] and the gas phase.[39] The UF_5 has generally been produced by photolysis of UF_6 with either a broad-band lamp[36,38] or a KrF (248 nm) laser.[39] (Codeposition of UF_4 and F_2 has also been used to produce UF_5 for matrix-isolation spectra[37]). The photofragment spectra taken by Kroger, Riley, and Kwei[40] show that photodissociation of UF_6 at 266 nm produces UF_5 with considerable internal energy (15–35 kcal/mol). They found a bimodal distribution in the UF_5 internal energy distribution as deduced from the F-atom translational energies. The two peaks occur at 1.0 and 1.4 eV with the former being more intense. There was not sufficient information to partition the internal energy into electronic and vibrational modes. However, the bimodal distribution is a strong indication that there are two different photodissociation channels producing UF_5 in different electronic states.[40]

The population of different electronic states is reasonable given the low-lying 5f states (below 15×10^3 cm^{-1}) in UF_5. It is not clear as yet which excited state (or states) of UF_6 is being excited in the photodissociation and so one cannot say which electronic states of UF_5 are being initially populated. Calculations in progress on the excited states of UF_6[17] should shed light on this process.

Nevertheless, the important point is that photolysis of UF_6 produces UF_5 with significant electronic and vibrational energy.[40] In the matrix isolation experiments, this excess energy will be rapidly dissipated into the matrix. However, in the gas phase at low pressures, the combination of the excess vibrational energy and the small barrier between the D_{3h} and C_{4v} structure means that the UF_5 will not have a well-defined geometry. This fluxional character together with the presence of multiple electronic states will greatly complicate the gas-phase infrared spectrum. In fact, the gas-phase infrared spectrum of UF_5 shows hot band features comparable to high-temperature UF_6 spectra, indicating the presence of many excited vibrational states.[39]

E. Environmental Effects on UF_5. One of the major goals of measuring the vibrational spectrum of UF_5 has been to determine its geometry. At first glance this appears straightforward since there are two infrared-active U–F stretching modes for D_{3h} and three for C_{4v}. The initial matrix isolation studies of Paine et al.[36] and Kunze et al.[40] revealed two bands at 560 and 584 cm^{-1} (for Ar matrix) in the U–F stretching region (500–650 cm^{-1}). The simplest conclusion might be that UF_5 is a trigonal bipyramid. However, the third U–F

stretching band for C_{4v} might be very weak or obscured by the UF_6 bands also present.

To elucidate the situation, Krohn et al.[41] calculated the intensities for the stretching bands in D_{3h} and C_{4v} based on a theoretical model, which had given good results for UF_6 and SF_6.[42] They found that the intensities of the two bands were consistent with a C_{4v} structure and that the third stretch was predicted to be very weak.[41] Their model assumed that the polar tensors for the axial and equatorial fluorines in UF_5 were basically the same. The present calculations give strong support to this assumption as demonstrated by the similarity of the Mulliken populations for D_{3h} and C_{4v} in Table VI.

More recently, Jones and Ekberg[38] have found a very weak band at 646 cm^{-1} for UF_5 in Ar matrices, which confirms the predictions of Krohn et al.[41] Using a force constant model to fit the wavelength and intensities of the U-F stretching bands, Jones and Ekberg[38] predict a C_{4v} geometry for UF_5 with an F_{ax}-U-F_{eq} angle of 101° and U-F_{ax} and U-F_{eq} bond lengths of 2.00 and 2.02 Å, respectively. These predictions are in excellent agreement with the equilibrium C_{4v} geometry predicted by the ab initio calculations (cf. Table I).

Taking the analysis of the vibrational spectra together with the present calculations allows one to conclude that the geometry of UF_5 in inert matrices is C_{4v}. Since the matrices should perturb the UF_5 weakly, one should be able to infer that the gas-phase structure of UF_5 is also square pyramid. However, one must check whether there is a significant differential effect on the D_{3h} and C_{4v} structures. The major difference between the two structures as to the effect of the matrix is that the C_{4v} structure has a nonzero dipole moment while the D_{3h} structure does not. The calculated dipole moment, μ, for the square pyramid is 1.88 D including spin-orbit coupling (The value is 1.93 D without spin-orbit effects.) This is a significant dipole moment. To estimate the stabilization of the UF_5 square pyramid in an inert matrix, one may use the model of a molecule in a spherical cavity of radius R (Å) surrounded by a dielectric medium with dielectric constant ϵ. The stabilization is given by[43]

$$\Delta E = 14.4\left(\frac{\epsilon - 1}{2\epsilon + 1}\right)\frac{\mu^2}{R^3} = 1.35\left(\frac{\epsilon - 1}{2\epsilon + 1}\right)$$

where we have chosen $R = 3.35$ Å $= 2.00 + 1.35 = R_{U\text{-}F} + R_F$ (van der Waals). Even in the limit of large dielectric constant, the stabilization is less than 1 kcal/mol. For inert matrices which have small dielectric constants, e.g., ϵ(liq Ar) = 1.54[44] and ϵ(liq He) = 1.056,[44] the stabilization is less than 0.2 kcal/mol.

The above arguments indicate that the equilibrium geometries for UF_5 in inert matrices and gas phase should be the same, namely, square pyramid. Nevertheless, direct determination of the gas-phase geometry will be very difficult given the fluxional nature of UF_5. To make a reliable gas-phase determination, UF_5 must be produced with very little excess internal energy (less than 1 kcal/mol). Photogeneration of UF_5 from UF_6 does not meet this criterion and so another approach must be determined or the excess energy must be removed, e.g., by adding an inert buffer gas.

Acknowledgments. The authors thank Richard Martin for helpful discussions. This work was performed under the auspices of the U.S. Department of Energy.

References and Notes

(1) M. S. Wrighton, *Chem. Rev.*, **74**, 401 (1974); M. A. Schroeder and M. S. Wrighton, *J. Am. Chem. Soc.*, **98**, 331 (1976); J. L. Graff, R. D. Sanner, and M. S. Wrighton, *ibid.*, **101**, 273 (1979).
(2) M. S. Wrighton, *Technol. Rev.*, **79** (6), 30 (1977); S. M. Kuznicki and E. M. Eyring, *J. Am. Chem. Soc.*, **100**, 6790 (1978).
(3) J. R. Bolton, *Science*, **202**, 705 (1978); G. Sprintschnik, H. W. Sprintschnik, P. P. Kirsch, and D. G. Whitten, *J. Am. Chem. Soc.*, **98**, 2337 (1976); K. R. Mann, N. S. Lewis, V. M. Miskowski, D. K. Erwin, G. S. Hammond, and H. B. Gray, *ibid.*, **99**, 5525 (1977); P. A. Grutsch and C. Kutal, *ibid.*, **99**, 646 (1977).
(4) (a) J. Demuynck, A. Strich, and A. Veillard, *Nouveau J. Chim.*, **1**, 217 (1977); (b) P. J. Hay, *J. Am. Chem. Soc.*, **100**, 2411 (1978).
(5) L. R. Kahn, P. J. Hay, and R. D. Cowan, *J. Chem. Phys.*, **68**, 2386 (1978).
(6) L. R. Kahn, P. Baybutt, and D. G. Truhlar, *J. Chem. Phys.*, **65**, 3827 (1976), and references cited therein.
(7) (a) W. C. Ermler, Y. S. Lee, and K. S. Pitzer, *J. Chem. Phys.*, **67**, 5861 (1977); (b) W. C. Ermler, Y. S. Lee, K. S. Pitzer, and N. W. Winter, *ibid.*, **69**, 976 (1978); (c) Y. S. Lee, W. C. Ermler, K. S. Pitzer, and A. D. McLean, *Ibid.*, **70**, 288 (1979); (d) W. C. Ermler, Y. S. Lee, and K. S. Pitzer, *ibid.*, **70**, 293 (1979).
(8) J. P. Desclaux, *At. Data Nucl. Data Tables*, **12**, 311 (1973); *Comput. Phys. Commun.*, **9**, 31 (1975).
(9) R. D. Cowan and D. C. Griffin, *J. Opt. Soc. Am.*, **66**, 1010 (1976)
(10) W. R. Wadt, P. J. Hay, and L. R. Kahn, *J. Chem. Phys.*, **68**, 1752 (1978).
(11) P. J. Hay, W. R. Wadt, L. R. Kahn, and F. W. Bobrowicz, *J. Chem. Phys.*, **69**, 984 (1978).
(12) W. R. Wadt, *Appl. Phys. Lett.*, **34**, 658 (1979).
(13) P. J. Hay, *J. Am. Chem. Soc.*, **100**, 2847 (1978).
(14) P. J. Hay, W. R. Wadt, L. R. Kahn, R. C. Raffenetti, and D. C. Phillips, *J. Chem. Phys.*, in press.
(15) H. A. Jahn and E. Teller, *Proc. R. Soc. London, Ser. A*, **161**, 220 (1937); A. D. Liehr, *J. Phys. Chem.*, **67**, 389 (1963); R. N. Porter, R. M. Stevens, and M. Karplus, *J. Chem. Phys.*, **49**, 5163 (1968); R. Englman, "The Jahn–Teller Effect in Molecules and Crystals", Wiley, New York, 1972.
(16) G. L. DePoorter and C. K. Rofer-DePoorter, *Spectrosc. Lett.*, **8**, 521 (1975); R. McDiarmid, *J. Chem. Phys.*, **65**, 168 (1976); W. B. Lewis, L. B. Asprey, L. H. Jones, R. S. McDowell, S. W. Rabideau, A. H. Zeltmann, and R. T. Paine, *ibid.*, **65**, 2707 (1976).
(17) P. J. Hay, unpublished results.
(18) C. Froese-Fischer, *Comput. Phys. Commun.*, **1**, 151 (1969); **4**, 107 (1972); **7**, 236 (1974); *J. Comput. Phys.*, **10**, 211 (1972).
(19) R. C. Raffenetti, *J. Chem. Phys.*, **58**, 4452 (1973).
(20) F. W. Bobrowicz and W. A. Goddard III in "Modern Theoretical Chemistry", Vol. III, H. F. Schaefer III, Ed., Plenum, New York, 1977. The SCF calculations were performed with the GVBTWO program of Bobrowicz and Wadt.
(21) W. J. Hunt and W. A. Goddard III, *Chem. Phys. Lett.*, **3**, 414 (1969).
(22) J. S. Cohen, W. R. Wadt and P. J. Hay, *J. Chem. Phys.*, in press.
(23) Since the pseudoorbitals do not have the proper behavior in the core region, they yield totally different expectation values for r^{-3}. Hence, Z_{iA}^{eff} no longer has the meaning of an effective charge, but is just an empirical parameter. See ref 14 for more details.
(24) C. E. Moore, "Atomic Energy Levels", Vol. I, *Natl. Bur. Stand. (U.S.), Circ.*, 467 (1958).
(25) M. Blume and R. E. Watson, *Proc. R. Soc. London, Ser. A*, **270**, 127 (1967).
(26) H. M. Seip, *Acta Chem. Scand.*, **19**, 1955 (1965).
(27) A. Messiah, "Quantum Mechanics", Vol. II, Wiley, New York, 1968, p 675.
(28) F. A. Cotton, "Chemical Applications of Group Theory", 2nd ed., Wiley, New York, 1971, p 289.
(29) For a complete listing of double groups and associated tables see: G. F. Koster, J. O. Dimmock, P. G. Wheeler, and H. Statz, "Properties of the Thirty-Two Point Groups", MIT Press, Cambridge, Mass., 1963.
(30) W. R. Wadt and W. A. Goddard III, *Chem. Phys.*, **18**, 1 (1976).
(31) P. Hafner and W. H. E. Schwarz, *J. Phys. B*, **11**, 2975 (1978).
(32) P. Hafner and W. H. E. Schwarz, *J. Phys. B*, **11**, 217 (1978).
(33) H. Maylotte, R. L. St. Peters, and R. P. Messmer, *Chem. Phys. Lett.*, **38**, 181 (1976).
(34) W. R. Wadt, unpublished results.
(35) A. Rosen and B. Fricke, *Chem. Phys. Lett.*, **61**, 75 (1979).
(36) R. T. Paine, R. S. McDowell, L. B. Asprey, and L. H. Jones, *J. Chem. Phys.*, **64**, 3081 (1976).
(37) K. R. Kunze, R. H. Hauge, D. Hamill, and J. L. Margrave, *J. Chem. Phys.*, **65**, 2026 (1976).
(38) L. H. Jones and S. Ekberg, *J. Chem. Phys.*, **67**, 2591 (1977).
(39) K. C. Kim, R. N. Fleming, and D. M. Seitz, *Chem. Phys. Lett.*, submitted for publication.
(40) P. M. Kroger, S. J. Riley, and G. H. Kwei, *J. Chem. Phys.*, **68**, 4195 (1978).
(41) B. J. Krohn, W. B. Person, and J. Overend, *J. Chem. Phys.*, **65**, 969 (1976).
(42) W. B. Person and J. Overend, *J. Chem. Phys.*, **66**, 1442 (1977).
(43) R. Huisgen, *Acc. Chem. Res.*, **10**, 117 (1977); K. J. Laidler and H. Eyring, *Ann. N.Y. Acad. Sci.*, **39**, 303 (1940).
(44) R. C. Weast, Ed., "CRC Handbook of Physics and Chemistry", 58th ed., CRC Press, Cleveland, p E-55.